AIAA AVIATION Forum
June 15-19, 2020, VIRTUAL EVENT
AIAA AVIATION 2020 FORUM

10.2514/6.2020-2515

The Effect of Shear Sheltering on Trailing Edge Noise

Ignacio Jimenez[1] and Stewart Glegg[2]
Department of Ocean and Mechanical Engineering, Florida Atlantic University, Boca Raton, FL 33431,USA

William J. Devenport[3]
Center of Research in Experimental Aero/hydrodynamic Technology (CREATe), Department of Aerospace and Ocean Engineering, Virginia Tech, Blacksburg, VA 2406, USA

Shear sheltering is defined as the effect of the mean flow velocity profile in a boundary layer on the turbulence caused by an imposed gust. It has been studied extensively in applications involving boundary layer transition, where the primary concern is flow instabilities that are enhanced by turbulence in the flow outside the boundary layer. In aeroacoustic applications turbulent boundary layers interacting with blade trailing edges or roughness elements are an important source of sound, and the effect of shear sheltering on these noise sources has not been studied in detail. Since the surface pressure spectrum below the boundary layer is the primary driver of trailing edge and roughness noise, we will consider the effect that shear sheltering has on the surface pressure spectrum below a boundary layer. We will model the incoming turbulence as vortex sheets at specified heights above the surface and show, using classical boundary layer profiles and approximations to numerical results, how the mean flow velocity can be manipulated to alter the surface pressure spectrum and hence the radiated trailing edge noise.

I. Introduction

Trailing edge noise occurs when turbulent flows within a boundary layer pass over a sharp trailing edge and is important in many applications, such as wind turbines, fan noise and airframe noise. Recent studies have demonstrated that trailing edge noise attenuation is possible using trailing edge devices such as those described by Clark *et al.* (2017). Numerical calculations related to the Clark *et al* experiment, such as the studies from Gonzalez *et al.* (2019) or Shi and Lee (2018), have shown that devices such as those used in Clark's experiments have a large impact on the mean velocity profile next to the surface. We will demonstrate in this paper that the mean velocity profile can be manipulated to reduce the surface pressure fluctuations at certain frequencies beneath a turbulent boundary layer, and hence reduce the associated radiated noise from trailing edges or surface roughness elements.

In the following sections we will first review past canopy flow studies that have shown that placing fine structures underneath the boundary layer of an incoming flow have an important effect on its mean velocity profile. We will then review the concept of shear sheltering and we will show that by imposing the condition that the velocity fluctuations for a fully developed turbulent boundary layer are stationary in time, and homogeneous in the streamwise and spanwise directions, the solutions to the Orr-Sommerfeld (OS) equation are effectively driven by a distribution of uncorrelated vortex sheets. Using this approach, we then use the solution to the OS equation to relate the surface pressure spectrum to a vorticity wavenumber spectrum and the mean flow velocity profile. The effect of shear sheltering can then be demonstrated using classical boundary layer profiles as well as an approximation of the modified boundary layer profiles that were calculated by Gonzalez *et al* (2019) and compare their pressure fluctuations against the pressure fluctuations from a linear mean velocity profile showing regions in the flow of high sensitivity and regions

[1] Graduate Research Assistant.
[2] Professor, Associate Fellow AIAA.
[3] Professor, Associate Fellow AIAA.

of low sensitivity due to shear sheltering or pressure shielding that would translate into a mitigation of trailing edge noise.

II. Background

The solution to the Orr Sommerfeld equation for the unsteady flow in a parallel two-dimensional shear flow is given by Grosch and Salwen (1978). For the case of a laminar boundary layer, they showed that there are a limited number of discrete modes in the solution, which decay exponentially with distance from the surface. In addition, a continuous spectrum was identified giving a solution that is bounded but does not decay to zero at large distances from the wall. It was subsequently shown by Jacobs and Durbin (1998) that the continuous spectrum decays rapidly within the boundary layer where the shear in the mean velocity profile is significant. This characteristic was later specified by Hunt and Durbin (1999) as shear sheltering. Most of the interest to study this phenomenon has been related to the effect of turbulence in the flow outside a laminar boundary causing instabilities prior to transition to turbulent.

In contrast, the interest of the study described herein is the effect of shear sheltering on the surface pressure spectra for fully developed turbulent boundary layers. The interest in this effect has been stimulated by the recent experimental work of Clark *et al* (2017) who showed that placing a canopy, or other such devices, beneath a fully developed turbulent boundary layer significantly reduced the surface pressure level. Clark *et al* (2017) also showed how the modified boundary layers reduced sound radiation from boundary layer turbulence incident on sharp trailing edges, or from roughness elements on the surface below the boundary layer. It should be noted that Clark's work was inspired by the paper by Lilley (1998) on the silent flight of the owl. The owl has small hairs on the surface of its feathers, and it was proposed by Lilley that this was a possible reason why the trailing edge noise from an owl's wing was reduced.

While the surface pressure spectrum is of primary interest in aeroacoustic applications it is also important in other engineering problems such as those that involve structural vibration or the performance of acoustic arrays. In the two-dimensional case, the surface pressure fluctuations are directly proportional to the flow speed close to the surface, so details of the surface pressure fluctuations beneath the atmospheric boundary layer are also relevant in assessing the effect of wind gusts on structures and plants Finnigan (2000) and Raupach *et al* (1996).

III. Theory/Approach

A. Trailing Edge Noise

Amiet (1975) showed that the far field noise from the trailing edge of an airfoil could be calculated from the surface pressure fluctuations caused by a turbulent boundary layer where the mean flow included embedded turbulence that caused a surface pressure fluctuation that is convected at uniform speed across the trailing edge. He also showed, as previously by Ffowcs-Williams and Hall (1969), that the direction of maximum sound radiation was normal to the span of the airfoil.

We will base our analysis on these principles and use the coordinate system seen in Fig. 1.

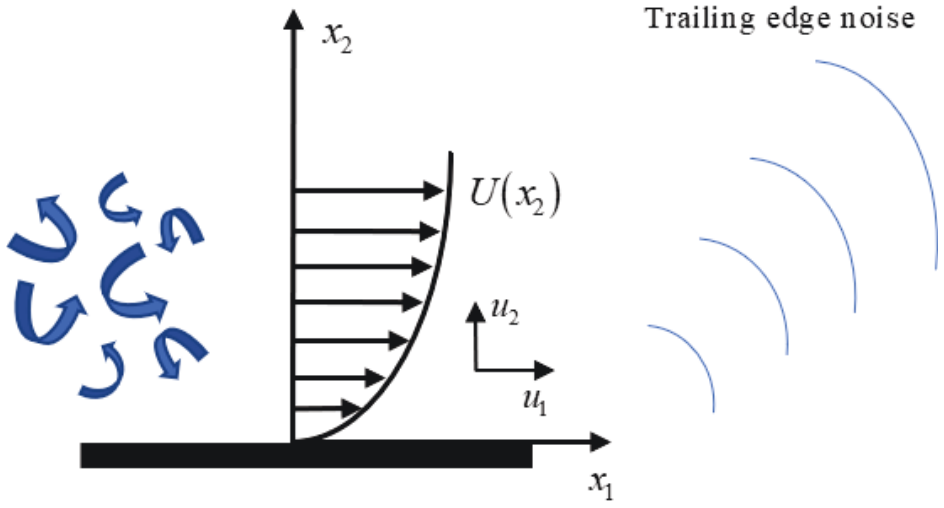

Fig. 1 Schematic of turbulence region showing the nomenclature for a flow passing over a trailing edge.

In Amiet's model the surface pressure was taken to be the superposition of waves with the time and space dependence exp($-i\omega t+ik_1x_1+ik_3x_3$) and it is shown in Glegg and Devenport (2017), section 15.2, that the far field sound in the plane normal to the span is determined solely by the wavenumber component $k_3=0$. Since this is the direction of maximum sound radiation it follows that, in order to study trailing edge noise, we can simply consider the surface pressure fluctuation being of the type exp($-i\omega t+ik_1x_1$). Therefore, we can model the flow as two dimensional. To verify that this argument is valid, we consider the Navier Stokes equations for a flow that has an unsteady velocity $u_i e^{-i\omega t+ik_1x_1}$ and a mean flow $U(x_2)$ in the streamwise direction x_1. If the mean flow terms are subtracted, the momentum equations yield

$$\begin{aligned}
&\frac{D_o u_1}{Dt}+u_2U'+\frac{ik_1p}{\rho_o}-\nu\left(u_1''-k_1^2u_1\right)=q_1\\
&\frac{D_o u_2}{Dt}+\frac{p'}{\rho_o}-\nu\left(u_2''-k_1^2u_2\right)=q_2\\
&\frac{D_o u_3}{Dt}-\nu\left(u_3''-k_1^2u_3\right)=q_3
\end{aligned}\tag{1}$$

where a prime represents a differentiation with respect to x_2, p is the pressure, ρ_o is the mean density, ν is the kinematic viscosity and D_o/Dt is the convective derivative linearized about the mean flow and for the harmonic gust defined above, yields $D_o/Dt\equiv -i\omega+ik_1U(y_2)=ik_1(U(y_2)-c)$, where $c=\omega/k_1$ is the phase speed of the gust. The terms on the right side of these equations, q_i, represent the non-linear terms and in linearized models these are set to zero. From the results in Eq. (1), we can state that the pressure fluctuations are only dependent on the spanwise unsteady velocity of the flow through the non linear terms. Therefore, if we ignore the nonlinear terms, a two dimensional model for the surface pressure is valid, even if the spanwise unsteady velocity is not zero.

B. Vorticity and Vortex Sheets

For the harmonic gust defined above, the continuity equation yields

$$ik_1u_1+u_2'=0$$

It follows from this that the unsteady velocity components and the spanwise vorticity are completely described by a stream function ψ defined such that

$$u_1=\psi' \qquad u_2=-ik_1\psi \qquad\qquad \omega_3=-\left(\psi''-k_1^2\psi\right)\tag{2}$$

and the vorticity equation yields

$$ik_1(U-c)\omega_3-u_2U''-\nu\left(\omega_3''-k_1^2\omega_3\right)=w_3\tag{3}$$

where the non-linear terms have been compacted to w_3.

In the linearized form of the vorticity equation we ignore both the viscous and non linear terms. This approximation is valid for high Reynolds number flows, for which the unsteady velocity u is small compared to the mean velocity. However, this approximation breaks down close to the wall and at the critical layer where the mean flow speed matches the phase speed so $U=c$.

Therefore, in the critical layer at a height y_c above the wall, we will model the non linear term using a vortex sheet located just above y_c at $x_2=y_c+d$, where d tends to zero. Since the layer is very thin, it will be modeled as a vortex sheet of strength $\Gamma_c\delta\left(x_2-\left(y_c+d\right)\right)$ that represents the viscous and non linear terms in Eq. (3) in the limit that d tends to zero. This disturbance, which drives the unsteadiness in the rest of the boundary layer at this frequency and wavenumber, is convected at the local flow speed that is equal to the phase speed $\omega/k_1=c$, and so is convected without amplification or distortion by the mean shear.

C. The Orr Sommerfeld Equation and its solution

To find a solution for the unsteady flow of an arbitrary mean flow profile we must eliminate the vorticity from Eq. (3) making use of the stream function, defined in Eq. (2) and replacing the vorticity and velocity terms. This leads to the well known Orr-Sommerfeld equation

$$(U(x_2)-c)\left(\psi''-k_1^2\psi\right)-U''(x_2)\psi=\frac{\nu}{ik_1}\left(\psi''''-2k_1^2\psi''+k_1^4\psi\right)+w_3\tag{4}$$

In the high Reynolds number limit $\nu=0$, so we can ignore the viscous terms, and if we assume the non linear terms w_3 are modeled by the vortex sheet, so $w_3=(U-c)\Gamma_c\delta(x_2-y_c)$, obtaining the inviscid form of this equation defined as,

$$\psi''-\left(\frac{U''}{U-c}+k_1^2\right)\psi=\Gamma_c\delta(x_2-y_c) \tag{5}$$

where y_c is the vortex sheet height in the limit that d tends to zero.

If we require the velocity to tend to zero at $x_2=\infty$ and $u_2=0$ on $x_2=0$, the solutions to this inviscid form of the OS equation are given by the Green's function

$$G(x_2;y_c)=\begin{Bmatrix}\dfrac{\psi_i(x_2)\psi_o(y_c)}{W} & x_2<y_c\\ \dfrac{\psi_o(x_2)\psi_i(y_c)}{W} & x_2>y_c\end{Bmatrix} \tag{6}$$

where ψ_i is the inner solution that satisfies the homogeneous and inviscid form of the OS equation and the boundary condition $\psi_i(0)=0$. The function $\psi_o(x_2)$ is the outer solution and W is the Wronskian defined as $W(x_2)=\psi_i\psi_o'-\psi_o\psi_i'$ which is a constant . The outer solution $\psi_o(x_2)$ matches the boundary condition as $x_2\to\infty$. If $U''(\infty)\to 0$, this requires that $\psi_o\sim Ae^{-k_1x_2}$ or $\psi_o'=-k_1\psi_o$ as $x_2\to\infty$.

The homogeneous solutions ψ_i and ψ_o are solutions to

$$\psi_{i,o}''-\left(\frac{U''}{U-c}+k_1^2\right)\psi_{i,o}=0 \tag{7}$$

This equation has a singularity at y_c where $U(y_c)=c$ and the two solutions in the vicinity of the singularity are known as the Tollmien's solutions ,as shown by Drazin and Reid (1981), and which are given by the expansion in powers of (x_2-y_c) as linear combinations of the two functions

$$\begin{aligned}\phi_1(\xi)&=\xi+\frac{U_c''}{2U_c'}\xi^2+\frac{1}{6}\left(\frac{U_c'''}{U_c'}+k_1^2\right)\xi^3\\ \phi_2(\xi)&=\frac{U_c''}{U_c'}\phi_1(\xi)ln(|\xi|)+1+\left\{\frac{U_c'''}{2U_c'}+\frac{(U_c'')}{(U_c')^2}+\frac{k_1^2}{2}\right\}\xi^2\end{aligned} \tag{8}$$

where $\xi=(x_2-y_c)$ and U_c',U_c'',U_c''' are derivatives of the velocity profile at $x_2=y_c$.

If the radius of convergence for this expansion extends to $x_2=0$, the inner solution must yield

$$\psi_i=\phi_1(\xi)\phi_2(-y_c)-\phi_2(\xi)\phi_1(-y_c) \tag{9}$$

so that the boundary condition is met at the wall.

For the outer solution, we choose a location $\xi=\xi_\infty$ where we require $\psi_o'=-k_1\psi_o$ and solve

$$\psi_o=\phi_1(\xi)-\alpha\phi_2(\xi) \tag{10}$$

for the constant α at the outer location, giving

$$\alpha=\left[\frac{\phi_1'+k_1\phi_1}{\phi_2'+k_1\phi_2}\right]_{\xi=\xi_\infty} \tag{11}$$

Therefore, we have all the parameters needed to calculate the Greens function defined in Eq. (6) that determines the total unsteady velocity of the flow ψ.

For the numerical computation, we start by calculating the coefficient $\dfrac{U''}{U-c}$ from the OS equation. We then compute the first, second and third derivative that are needed for the analytical Tollmien's solution from Eq. (8). We then use the analytical Tollmien's solution in Eq. (8) for the unsteady velocity in the region close to the vortex sheet as the initial conditions for the numerical integration that uses Euler's method going inwards and outwards from the critical layer computing ϕ_1 and ϕ_2, and then use Eqs. (9)-(11) to obtain ψ_i and ψ_o.

In order to have a baseline result that will be used as comparison for all the other cases as well as proof of the legitimate use of the numerical solutions, we start by studying the simple monotonically increasing mean velocity profile in Fig. 2. This mean velocity profile is normalized on the phase speed that equals the mean velocity at the specific non dimensional vortex height selected. For this profile we have an analytical solution for the unsteady velocity that can be used to scrutinize the numerical model and is given by

$$G(x_2; y_c) = \begin{cases} \dfrac{sinh(k_1 x_2)\, e^{-k_1 y_c}}{-k_1} & x_2 < y_c \\ \dfrac{e^{-k_1 x_2}\, sinh(k_1 y_c)}{-k_1} & x_2 > y_c \end{cases} \tag{12}$$

Figure 2 (Right) shows the convergence between the analytical and numerical solution of the unsteady velocity for the linear mean velocity profile in Fig. 2 (Left). The solution of this ideal profile will be used as baseline for comparison against the solutions obtained from more complicated profiles where $D_o\omega_3/Dt \neq 0$.

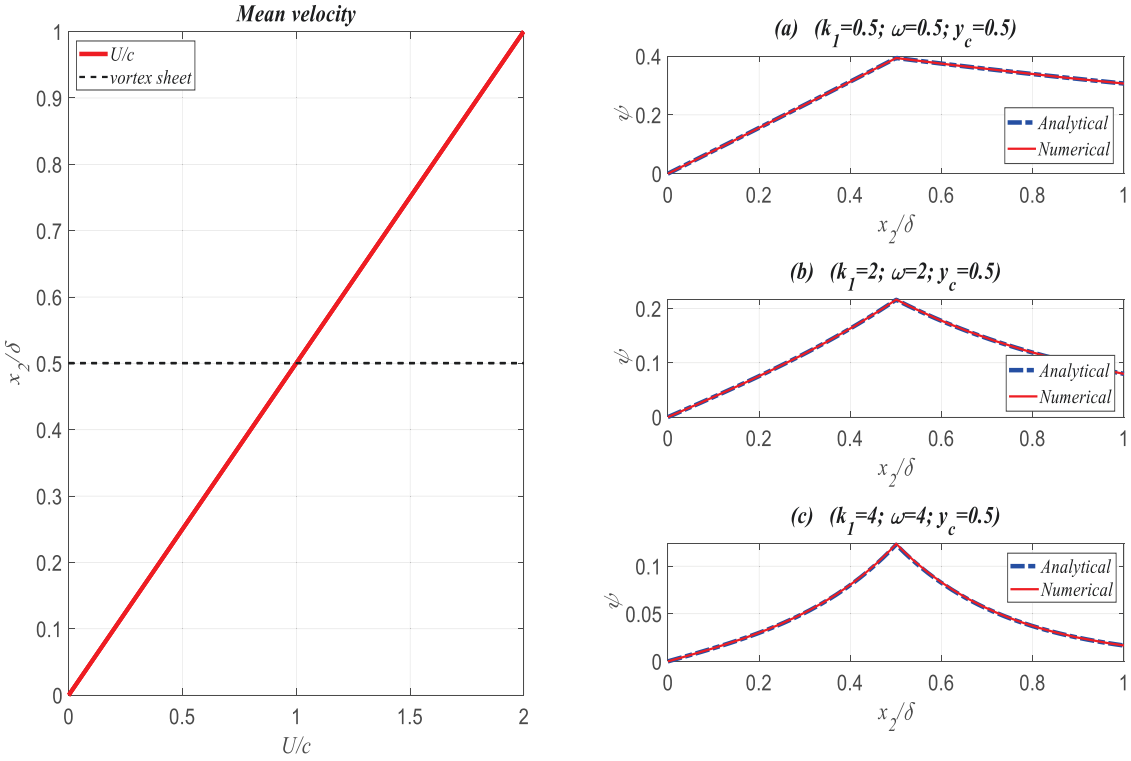

Fig. 2 (Left) Linear mean velocity profile with vortex sheet. (Right) Magnitude of ψ for linear mean velocity profile at three different non dimensional frequencies.

First, we study a classic zero pressure gradient turbulent boundary layer profile that is defined by the log law as

$$u^+ = \frac{1}{\kappa} \ln x_2^+ + C$$

where the values of the von Kármán constant κ and the constant C are chosen to be 0.4 and 4.9 respectively.

The mean velocity profile is then characterized as in Fig. 4 (Left), using a typical boundary layer thickness of 10000 wall units and the free stream velocity of U_m. Fig. 3 shows a comparison of the turbulence level that would be obtained from this mean velocity profile against the turbulence level from the linear mean velocity profile shown in Fig. 2 (Left). From the results, we see that changing the mean velocity profile has a large impact on the unsteady velocity of the flow and this effect is more evident for the streamwise component u_1. It is noteworthy the big response of the streamwise unsteady component of the velocity at the vortex sheet, decays to zero with distance inward and outward from the vortex sheet.

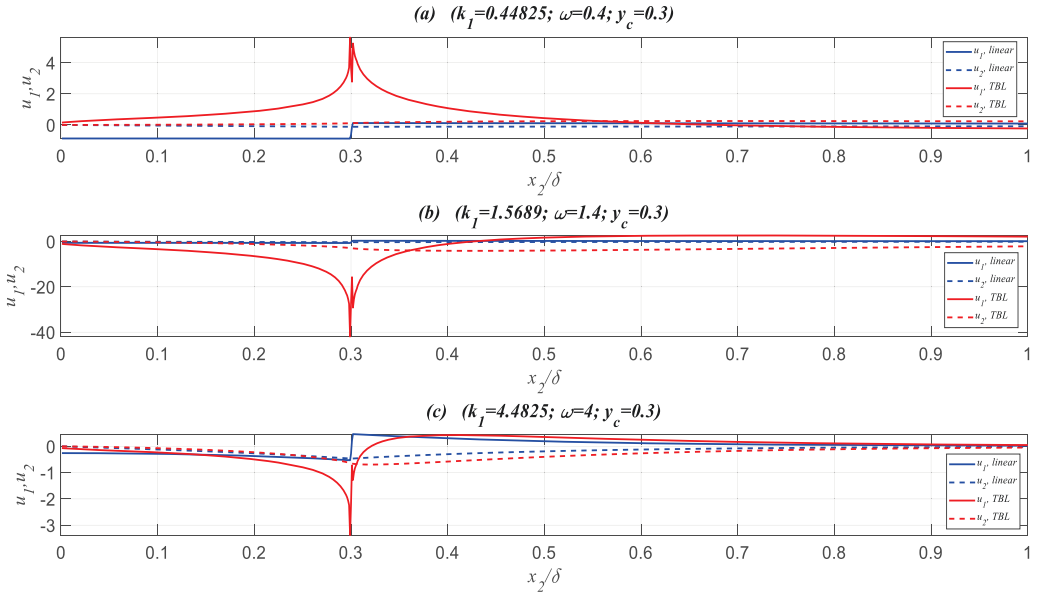

Fig. 3 Magnitude of unsteady velocity component u_1 and u_2 of TBL compared to linear profile.

Figure 4 (Right) is a comparison of the stream function that would be obtained from the same turbulent boundary profile shown in Fig. 4 (Left). From the results, we see that changing the mean velocity profile also has a large impact on the u_2 component of the unsteady flow and this effect is more evident at some particular frequencies. Note, in the following figures we present the stream function ψ to describe the unsteady flow because it is proportional to $u_2 = -ik_1\psi$. Furthermore, it is important to note that for this study we fixed the vortex sheet strength Γ_c of every profile so that the jump in velocity across the sheet depends only on the local mean velocity profile.

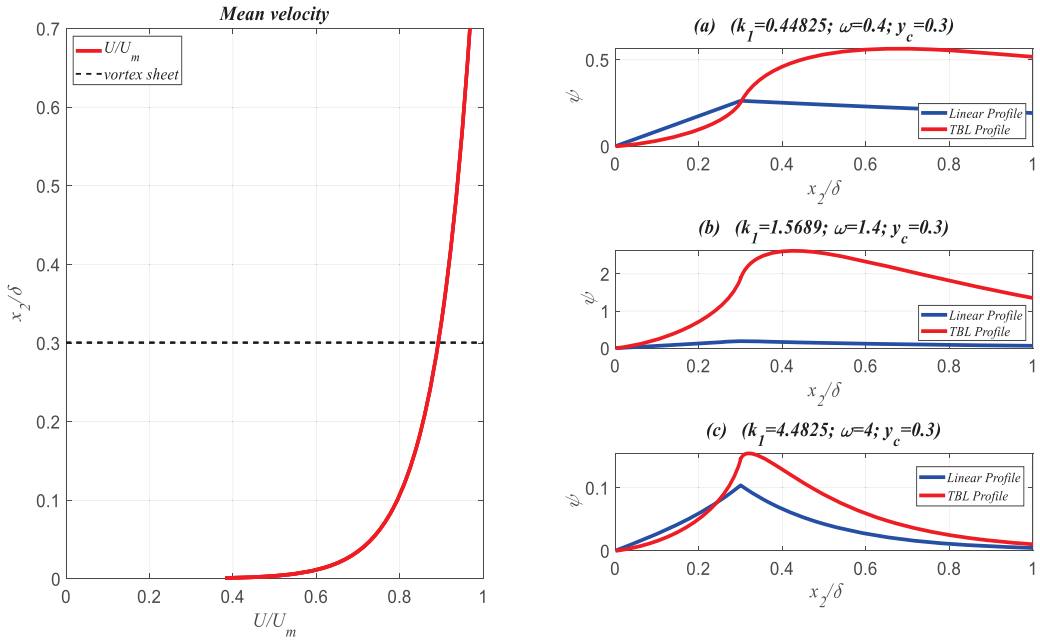

Fig. 4 (Left) Turbulent Boundary Layer Mean Velocity Profile with vortex sheet. (Right) Magnitude of ψ for linear and TBL mean velocity profile at three different non dimensional frequencies.

The second profile studied is shown in Fig.5 (Left). Defined as $U(x_2) = 1 - e^{-\beta x_2}$, where $\beta = 1$,which is more typical of a laminar boundary layer. It can be seen from results in Fig.5 (Right), that at some frequencies, the unsteady velocity decays more rapidly in the region below the vortex sheet compared to the unsteady velocity solution above the vortex sheet. This phenomenon is what Jacobs, Hunt and Durbin called shear sheltering since the mean velocity profile with greater shear, reduces the turbulence level under the vortex sheet. However, there are frequencies that show an enhancement of the turbulence level compared to the baseline profile as seen from the result in Fig. 5 (Right, (b)) where ψ in the region underneath the vortex sheet is greater for the linear profile, enhancing the turbulence level in that region. We will define this effect as shear amplification.

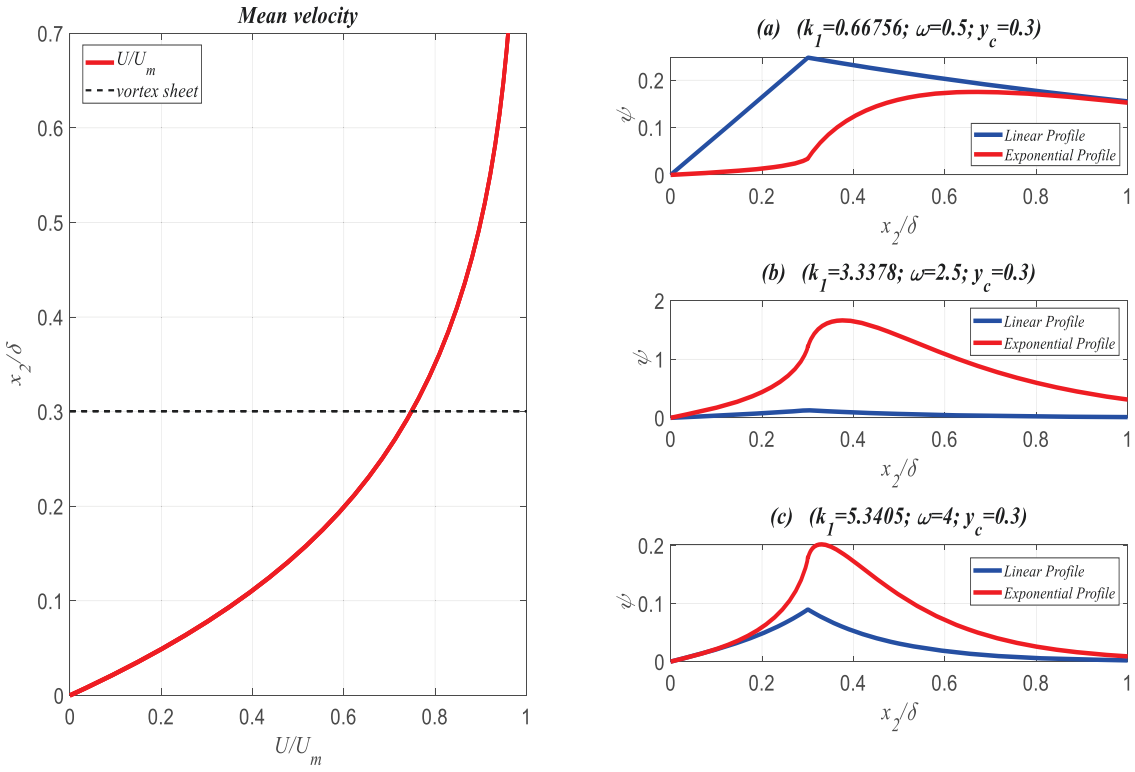

Fig. 5 (Left) Exponential Boundary Layer Mean Velocity Profile with vortex sheet. (Right) Magnitude of ψ for linear and exponential mean velocity profiles at three different non dimensional frequencies.

Another profile of interest in this study is the one shown in Fig. 6 (Left). This profile is an approximation of the results that were recorded in experiments of vegetation canopies conducted by Raupach *et al.* (1996) and Finnigan (2000). In these experiments, they recorded the mean velocity of different flows that encounter a vegetation canopy. The scenarios they studied varied from wheat crops, forest and also emulated indoor experiments. In all the scenarios, they recorded a velocity profile similar to the one shown in Fig. 6 (Left).

Using this profile in our model, shows that the inflected mean velocity profile has a great impact on the unsteady velocity of the flow. Fig. 6 (Right, (a)) shows a lower level of ψ under the vortex sheet for this mean velocity profile at a low frequency compared to the decay that would be obtained from the linear profile in Fig. 2 (Left). Therefore, the rate of change of ψ is smoother in the region underneath the vortex sheet translating into shear sheltering. However, there are some frequencies like the one seen in Fig. 6 (Right, (b)) that show a much greater level of ψ under the vortex sheet compared to the linear profile. This would lead to shear amplification instead of sheltering. Furthermore, the amplitude of ψ is greatly enhanced at this particular frequency and vortex sheet height that corresponds to the inflectional point of the mean velocity profile. This shows that some profiles are more easily excited than others at certain frequencies. By exciting a boundary layer like the one on Fig. 6 (left) at the inflectional point, you get as a result a large unsteady velocity response. This is a reflection of the inherent instability of an inflected mean velocity profile in the onset of Kelvin Helmholtz waves. Finally, Fig. 6 (Right, (c)) shows the solution of ψ at

a higher frequency. At this high frequency, the impact of the mean velocity profile is not as noticeable as at the other frequencies. The value of ψ is very similar for both solutions.

Hence, we see that in general, the effect of the mean velocity profile is more pronounced at the lower frequencies.

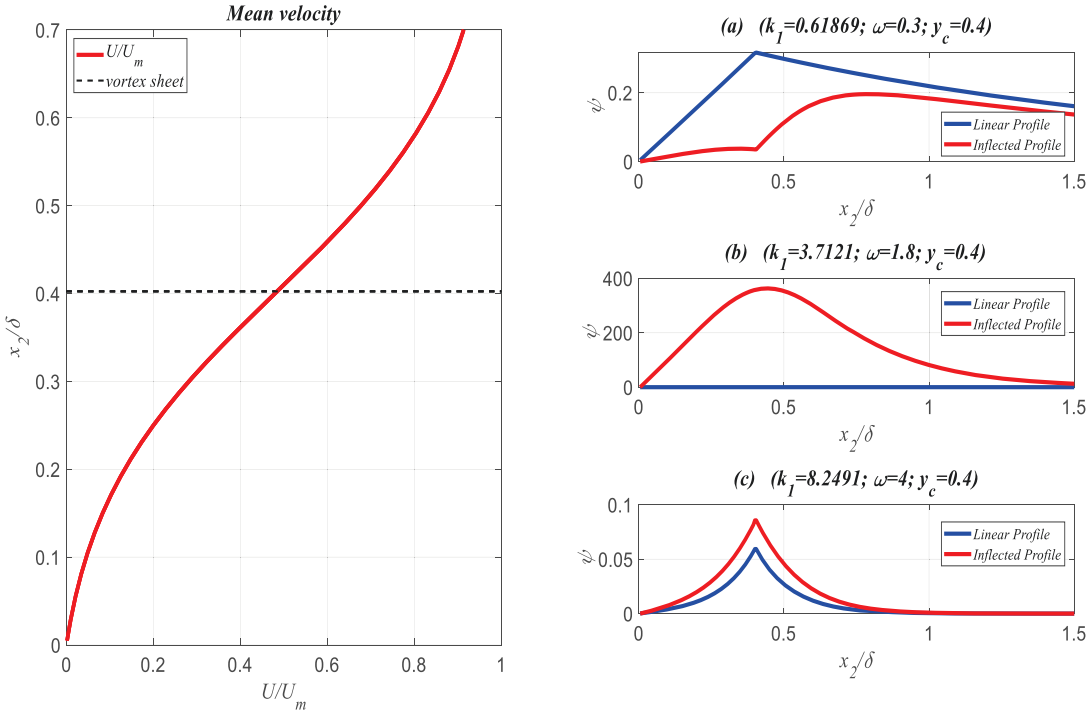

Fig. 6 (Left) Approximation to vegetation canopy boundary layer with vortex sheet. (Right) Magnitude of ψ for linear and inflected mean velocity profiles at three different non dimensional frequencies.

The bio inspired Trailing-Edge Noise Control study conducted by Clark *et al.* (2017) has been the motivation to understand the details intrinsic to the analysis of canopy flows. Gonzalez *et al* (2019) performed a RANS analysis on a noise reduction experiment inspired by Clark *et al.* (2017) findings. In this experiment, Gonzalez *et al.* simulated the wall jet flow passed a smooth flat plate that was covered by a structure of fine steel rods at a height of h=4 mm from the smooth wall. These rods were placed in an attempt to mimic the anatomical structure of an owl's feathers. In those simulation, Gonzalez *et al.* found that placing the rod canopy over the smooth wall not only helped in reducing the far field noise but also lifted the turbulent kinetic energy above the wall as previously seen by Bodling and Sharma (2018). It also had an important effect in the mean velocity profile of the wall jet flow in a region close to the wall where the canopy was located as a result of aerodynamic drag.

Figure 7 (Left) is an approximation of that mean velocity profile simulated by Gonzalez *et al.* Using this profile in our model of the unsteady velocity allows us to compare the solutions to the ones that would be obtained from the linear profile as seen in Fig. 7 (Right) for a specific vortex height selected and for three different nondimensional frequencies. Fig. 7 (Right, (a)) shows again how the shear of the mean velocity profile has an effect on the unsteady part of the velocity, decaying much more rapidly in the region underneath the vortex sheet and maintaining an almost horizontal slope of ψ in this region. The maximum of ψ at this frequency is slightly above the vortex sheet height and one oscillation occurs before it decays to zero with distance from the wall. Fig. 7 (Right (b)) shows the solution of ψ at a different frequency. In this case, the maximum of ψ again occurs slightly above the vortex sheet height, however this time there is an oscillation going outwards from the wall but also an oscillation going inwards in the region underneath the vortex sheet. This oscillation makes the rate of change of ψ in this region much greater than the rate of change that would be seen from a linear profile translating into shear amplification from this mean velocity profile at this particular frequency if the vortex sheet is located at the selected height. Finally, Fig. 7 (Right, (c)) shows something that has not been seen for the previous mean velocity profiles. At that particular frequency, the maximum of ψ occurs slightly below the vortex sheet, however above the vortex sheet, the solution remains almost constant and very close to zero.

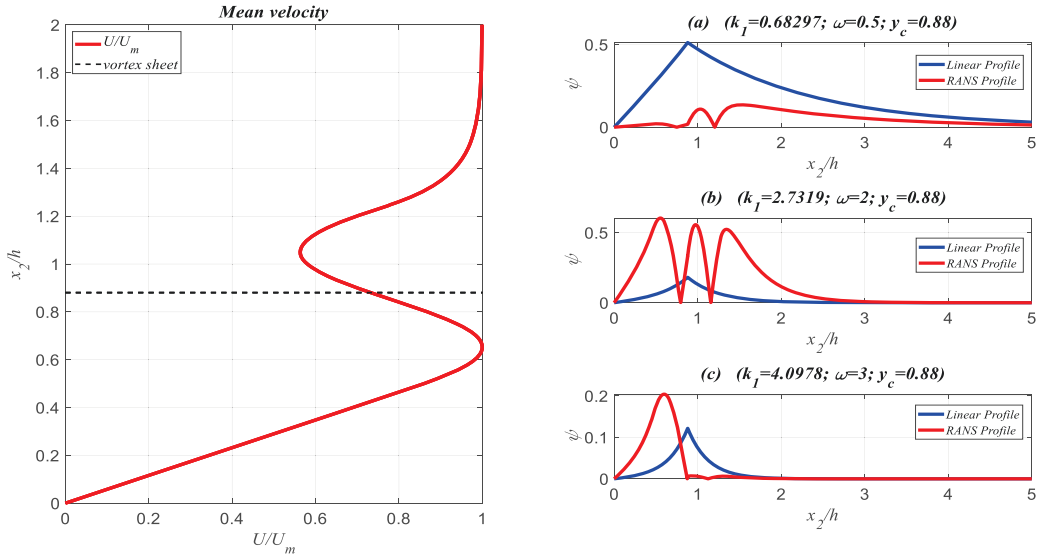

Fig. 7 (Left) Approximation of Gonzalez *et al.* RANS mean velocity profile with vortex sheet. (Right) Magnitude of ψ for linear and RANS mean velocity profiles at three different non dimensional frequencies.

The results from these profiles, demonstrate that the mean velocity has an impact on the unsteady part of the flow. The solution of ψ gets affected depending on the shape of the mean velocity profile. This translates into different turbulence levels for flows with different mean velocity profiles.

D. The Surface Pressure

Determining the unsteady velocity is crucial on the study of surface pressure fluctuations which are the source of trailing edge noise. In fact, we can use the results from the previous section to obtain the surface pressure fluctuations at $x_2 = 0$ directly from the momentum equation which gives, in the inviscid limit,

$$ik_1(U-c)u_1 + k_1u_2U' + \frac{ik_1p}{\rho_0} = 0 \tag{13}$$

and since both U and u_2 are zero on the surface we obtain

$$p_s = \rho_0 c \left| \frac{\partial \psi}{\partial x_2} \right|_{x_2=0} \tag{14}$$

Implementing the solution of the OS equation,

$$p_s = \rho_0 c \Gamma_c \frac{\psi_i'(0)\psi_o(y_c)}{W}$$

where W is the Wronskian defined as

$$W = \psi_i(x_2)\psi_o'(x_2) - \psi_i'(x_2)\psi_o(x_2) = const$$

Therefore, setting $x_2 = 0$ gives

$$W = -\psi_i'(0)\psi_o(0)$$

Hence, the surface pressure fluctuations will be defined as

$$p_s = -\frac{\rho_0 c \Gamma_c \psi_o(y_c)}{\psi_o(0)} \tag{15}$$

This solution is the one used for the results of this study and it was shown numerically to be identical to the one that would be obtained if we had taken the divergence of the momentum equation to find a Poisson's equation that would yield to the solution defined us

$$p_s = -2k_1 \int_0^\infty U'(x_2)\psi(x_2)e^{-k_1x_2}dx_2 \tag{16}$$

However, this integral only converges slowly at low frequencies and so Eq. (15) was found to be preferable providing more consistent results. In order to interpret the results of the surface pressure fluctuations spectra as a function of vortex height and frequency, we use the sheltering attenuation coefficient that is defined as

$$F = -20\log_{10}\left(\frac{p_s(\omega, y_c)}{p_{s,o}(\omega, y_c)}\right) \tag{17}$$

where $p_s(\omega, y_c)$ are the surface pressure fluctuations resulting from any specific mean velocity profile and $p_{s,o}(\omega, y_c)$ are the surface pressure fluctuations resulting from the linear mean velocity profile from Fig. 2 (Left). Therefore, when the sheltering attenuation coefficient is a large positive number, there is a region of low sensitivity and pressure shielding takes place. However, regions where the sheltering attenuation coefficient is a large negative number, corresponding to a region of high sensitivity where the effect of the mean velocity profile will impact the unsteady velocity causing shear amplification and the surface pressure fluctuation could increase.

IV. Results

The far field noise produced at the trailing edge of an airfoil depends on the surface pressure spectrum of the incoming turbulent boundary layer and using the models described we can study the effect of different velocity profiles on the radiated trailing edge noise by considering the effect that the mean velocity profile has on the surface pressure fluctuations.

We utilize the sheltering attenuation coefficient defined in Eq. (17) that compares the surface pressure fluctuations obtained from any particular mean velocity profile to a baseline pressure spectrum obtained from a linearly increasing mean velocity profile.

We first study the pressure spectrum that would be obtained from the turbulent boundary layer profile shown in Figs. 4 and 8 (Left). We use the sheltering attenuation factor defined in Eq. (17) and compare the sound pressure level that would be obtained from the turbulent profile to the sound pressure level that would be obtained from the ideal linear profile.

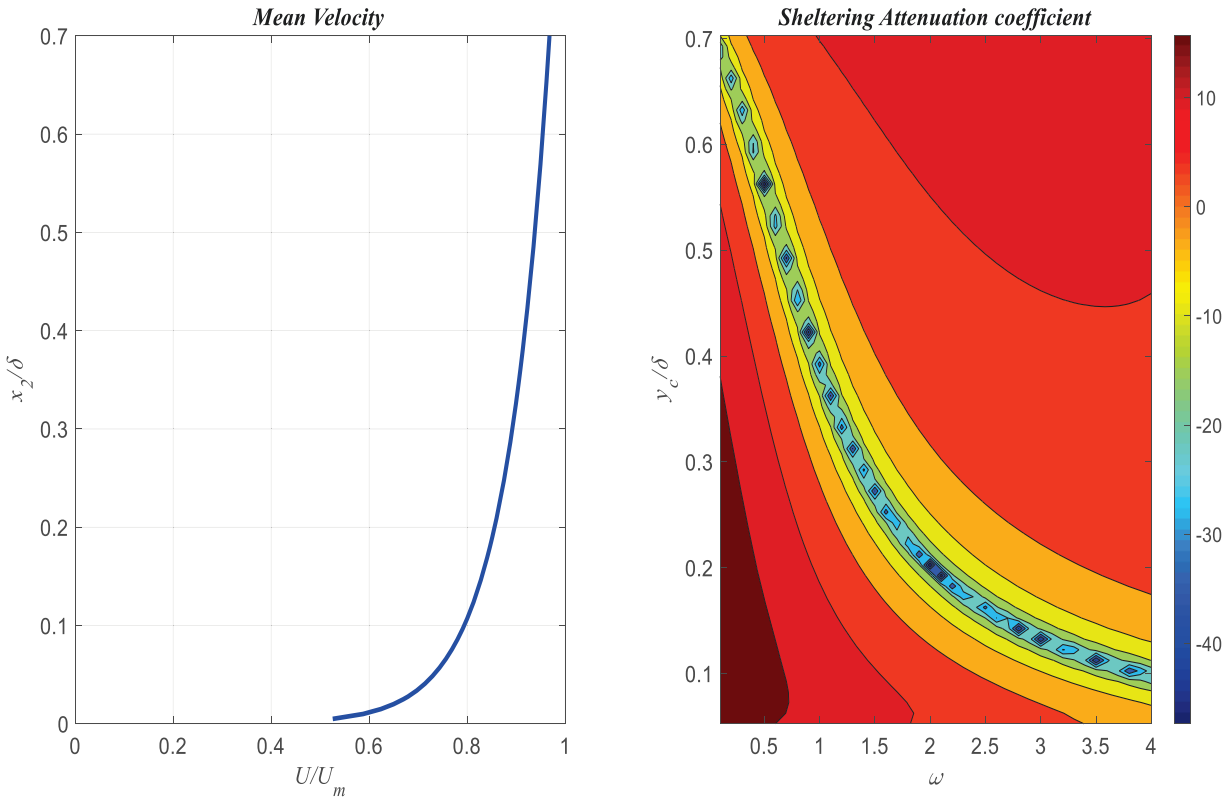

Fig. 8 (Left) Turbulent Boundary Layer Mean Velocity Profile. (Right) Sheltering Attenuation Coefficient for TBL velocity Profile.

The results of this comparison are presented in the contour in Fig 8. (Right) where the vortex sheet heights go from $y_c/\delta = 0.05$ to $y_c/\delta = 0.7$.

The negative values of the sheltering attenuation coefficient correspond with a region of high sensitivity and is furthest from the wall at low frequencies and very close to the wall at higher frequencies, as expected from classical experimental observations of turbulent flows.

In order to explain the low and high sensitivity regions from the contours, we consider the integrand of the pressure definition from Eq. (16) that can be defined as $I = U'(x_2)\psi(x_2)e^{-k_1 x_2}$ and that it is shown in Fig. 9 (Right) for the turbulent boundary layer profile in comparison to the result for the linear profile. If the area under the function *I* is smaller for each of the mean velocity profiles of study than the area of *I* for the linear profile, the surface pressure fluctuations will be less prominent and pressure shielding could be accomplished. This is very clear for the turbulent boundary layer at the frequency selected in Fig. 9 (Right, (a)) which corresponds to a region in the contour of Fig. 8 (Right) of low sensitivity.

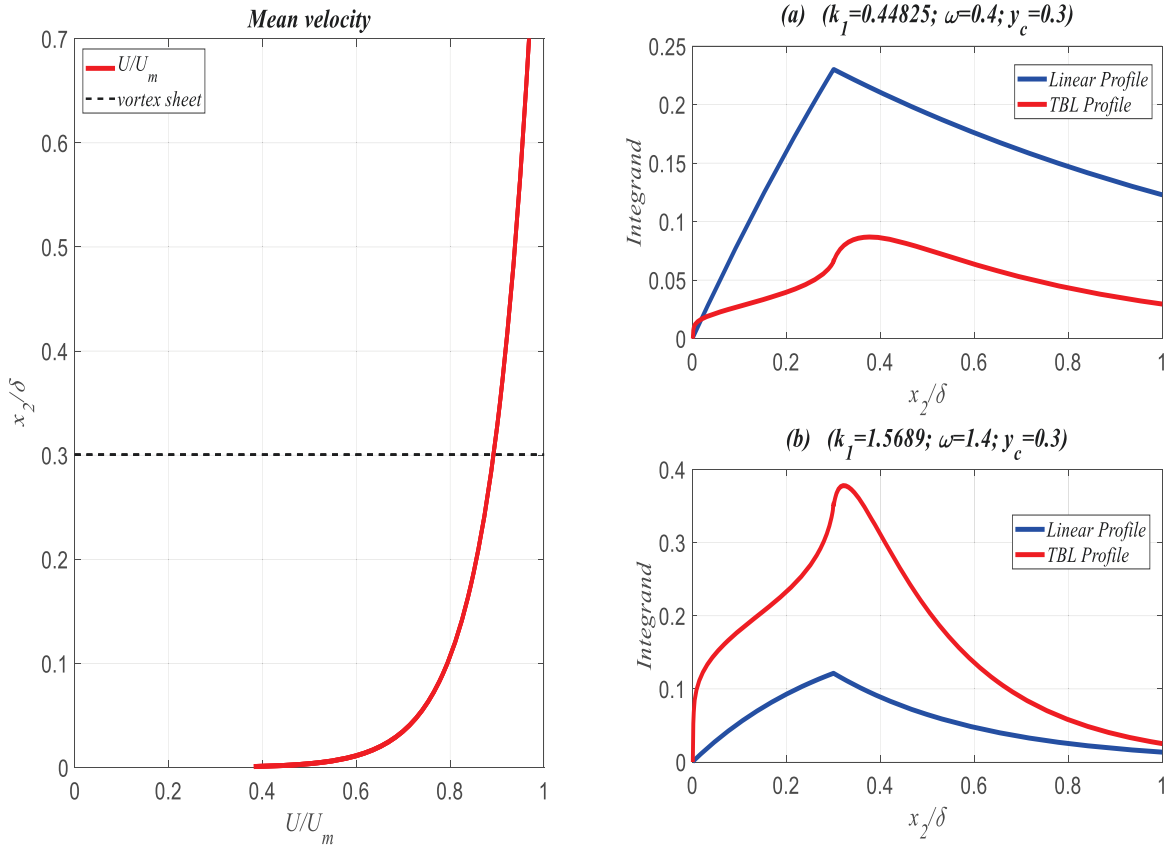

Fig. 9 (Left) Turbulent Boundary Layer Mean Velocity Profile with vortex sheet. (Right) Magnitude of the Integrand *I* from surface pressure definition.

However, if we look into a frequency inside the band of high sensitivity for this specific vortex height as it is shown in Fig. 9 (Right, (b)), the area under the function *I* for the turbulent boundary layer is much greater than the area under the function *I* that would be obtain from the linear mean velocity profile. Therefore, from the definition of Eq. (16), the surface pressure fluctuations will be enhanced at that particular frequency explaining the high sensitivity from the contour.

If we look at the exponential mean velocity profile shown in Fig. 10 (Left), which is the same as in Fig. 5 (Left), the results of the sheltering attenuation coefficient drastically change compared to the results from the turbulent boundary layer due to a completely different surface pressure spectrum obtained from this profile. For the exponential velocity profile, we see a reversal in the contour of Fig. 10 (Right). Unlike the surface pressure spectrum from the logarithmic turbulent boundary layer profile, for this case the region of high sensitivity is closest from the wall at the low frequencies and very far from the wall at higher frequencies.

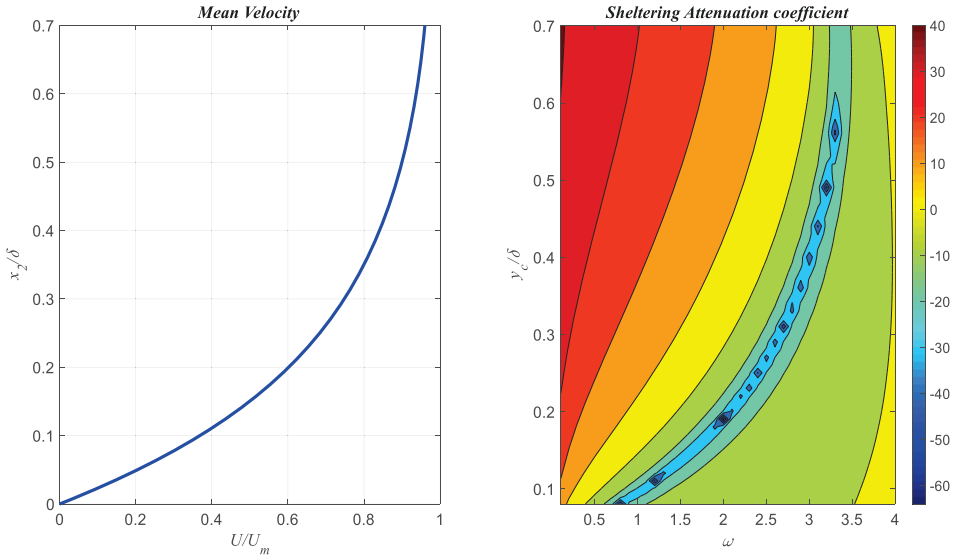

Fig. 10 (Left) Exponential Boundary Layer Mean Velocity Profile. (Right) Sheltering Attenuation Coefficient for exponential velocity Profile.

The regions of low and high sensitivity can again be explained comparing the area under the function *I* for the Exponential profile in comparison to the area under the function *I* that would be obtained from a linear mean velocity profile. Fig. 11 (Right, (a)) shows a frequency of low sensitivity at the selected vortex sheet height where the area under the integrand is much lower for the exponential profile than for the linear profile. On the other hand, Fig. 11 (Right, (b)), shows a frequency of high sensitivity where indeed the area under the integrand of the exponential profile is much greater than the area under the integrand of the linear profile translating into high sensitivity. It is noteworthy that, in this case the area that causes most of the pressure fluctuations on the surface is just above the vortex sheet, and is much more pronounced than for the TBL case shown in Fig. 9.

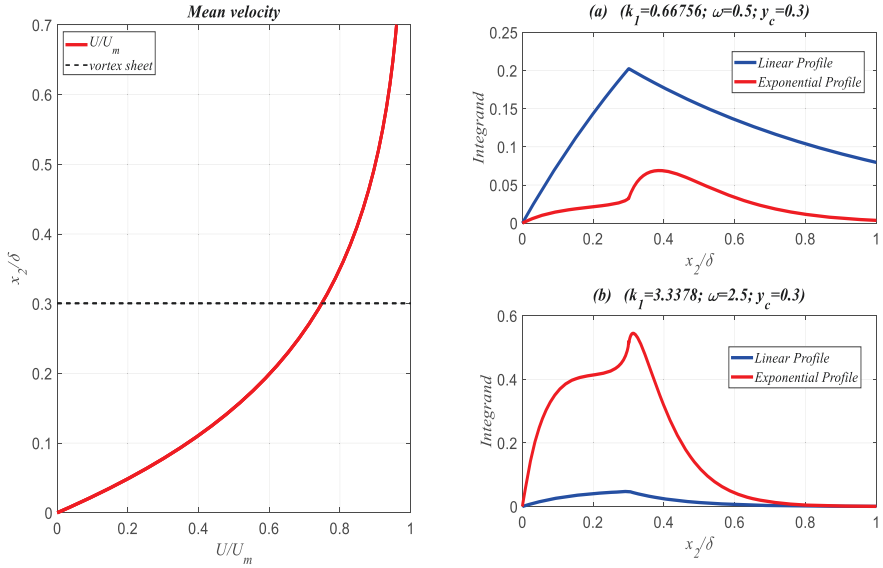

Fig. 11 (Left) Exponential Boundary Layer Mean Velocity Profile with vortex sheet. (Right) Magnitude of the Integrand *I* from surface pressure definition.

The next profile of study is the approximation to vegetation canopy boundary layers in Fig. 12 (Left). Analyzing the sheltering attenuation coefficient of this profile in Fig. 12 (Right), we see a similar result to the one obtained from the Exponential mean velocity profile in Fig. 10 (Right). However, there is a greater region of low sensitivity due to shear sheltering that is especially noticeable further away from the wall and that would translate into pressure shielding. Furthermore, the band of high sensitivity has a different curvature to the one obtained from the exponential

profile since due to shear sheltering, the region of high sensitivity is closer to the wall at the higher frequencies compared to the results obtained from the exponential profile. There is also a peak of high sensitivity at non dimensional frequencies between $\omega = 1.5$ and 2. This high sensitivity peak is coming from the vortex height of $y_c / \delta = 0.4$ which correspond to the inflectional point of the mean velocity profile.

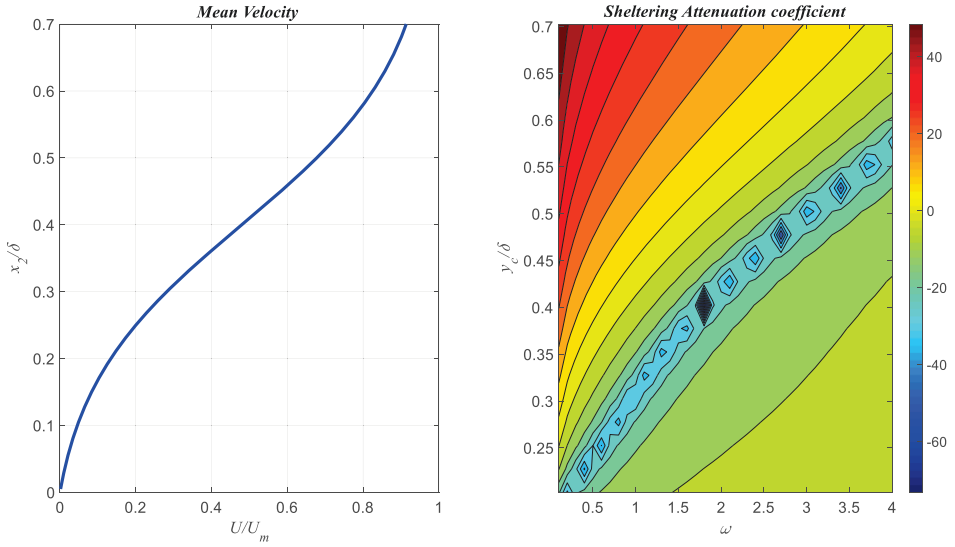

Fig. 12 (Left) Approximation to vegetation canopy boundary layer mean velocity profile. (Right) Sheltering Attenuation Coefficient for approximation of vegetation canopy mean velocity profile.

Figure 13 (Right, (b)) explains that peak of high sensitivity, at that particular frequency and particular vortex height, the amplitude of the integrand function *I* resulting from the inflected profile in Fig. 13 (Left) has a very large area in comparison to the integrand function from the linear profile. Therefore, the surface pressure fluctuations generated at the location of the inflectional point from this mean velocity profile would have a very high impact compared to the pressure fluctuations that would be seen if we place that vortex sheet source at the same height but in a linear profile.

However, at this same vortex sheet height, but at a lower frequency where we see low sensitivity in the contour, the area of the integrand will be smaller for the inflected profile than for the linear profile as seen in Fig. 13 (Right, (a)), resulting in pressure shielding.

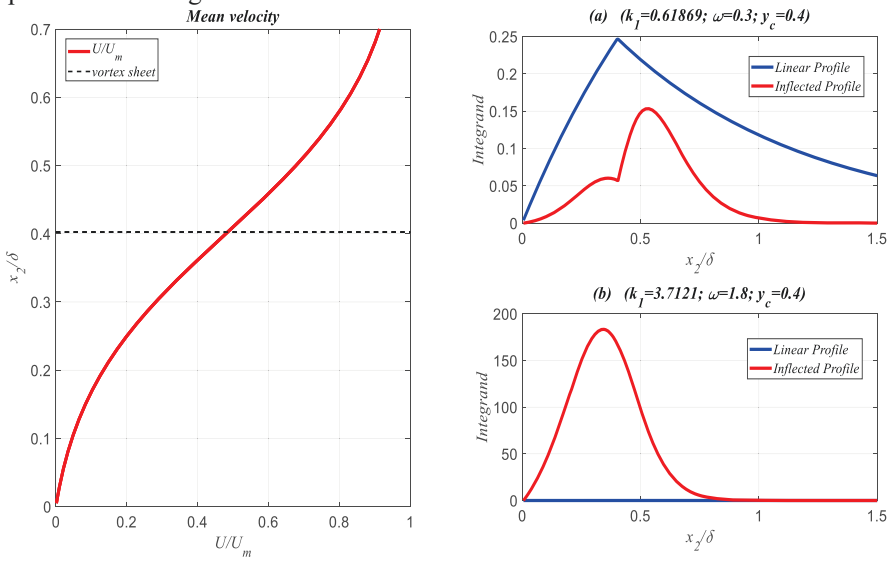

Fig. 13 (Left) Approximation to vegetation canopy boundary layer mean velocity profile with vortex sheet. (Right) Magnitude of the Integrand *I* from surface pressure definition.

Of particular interest is the mean velocity profile in Fig. 14 (Left) which is the approximation of the simulation results obtained by Gonzalez *et al.* that were based on bio inspired experiments motivated by the discoveries by Clark *et al.*

Performing the same analysis as with the other profiles, the contour on Fig. 14 (Right) shows two regions of very low sensitivity due to shear sheltering that correspond to the maximum and minimum of the mean velocity profile. Furthermore, there is a large band of low sensitivity that starts under the minimum of the mean velocity profile at x_2/h of about 1.05 for very low frequencies and extends in frequency as the vortex sheet is moved inwards towards the wall for vortex heights of y_c/h between 0.5 and 0.85 and non dimensional frequencies from 0.1 to 2. However, there are also large regions of frequencies with high sensitivity where the sheltering attenuation coefficient becomes negative as seen from the dark blue regions in the contour of Fig. 14 (Right).

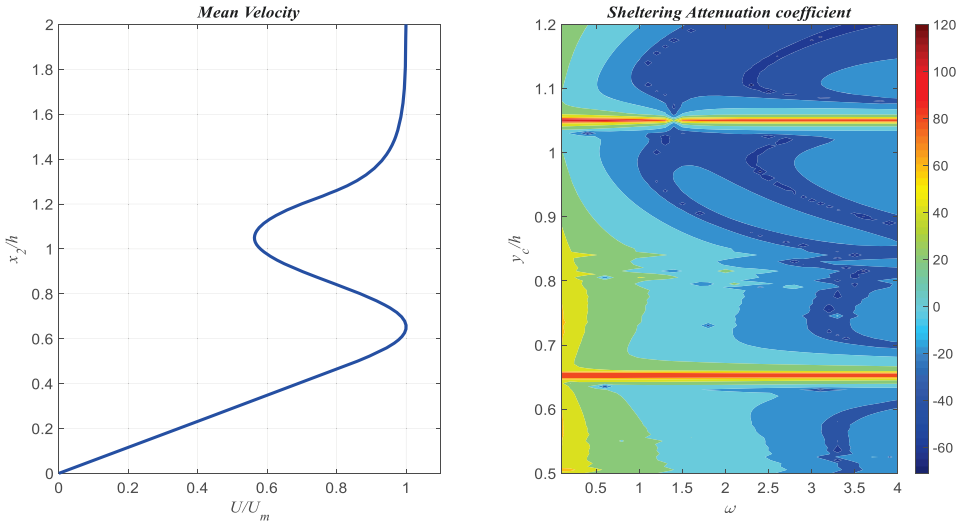

Fig. 14 (Left) Approximation of Gonzalez et al. RANS mean velocity profile. (Right) Sheltering Attenuation Coefficient for approximation of RANS mean velocity profile.

Selecting a vortex height as shown in Fig. 15 (Left) shows the effect of the mean flow just below the height of the canopy would have compared to the linear profile. Fig. 15 (Right,(a)) shows a frequency of low sensitivity where the area under the integrand is greatly reduced compared to the area under the linear integrand. Fig. 15 (Right,(b)) shows a high sensitivity frequency for the selected vortex height where the area under the integrand is greater than for the linear profile.

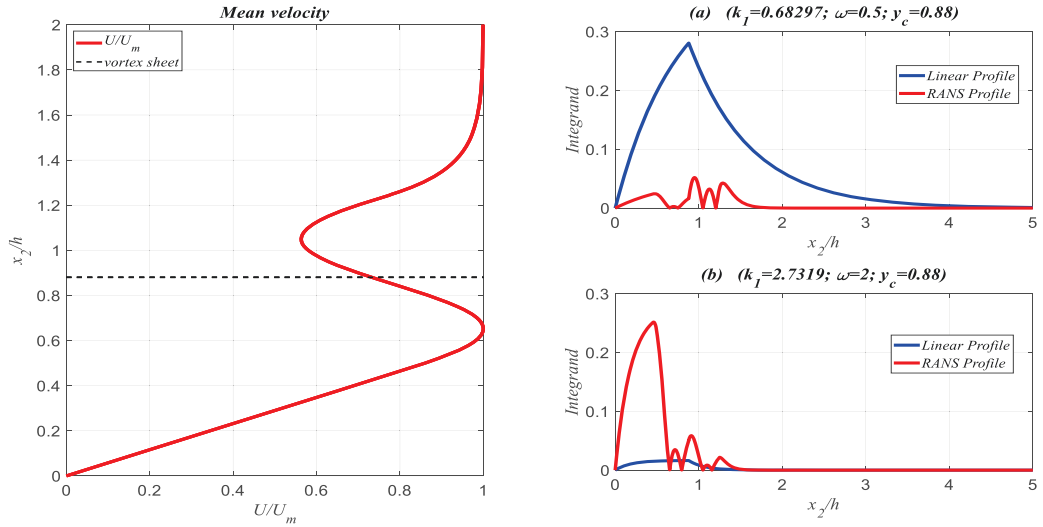

Fig. 15 (Left) Approximation of Gonzalez et al. RANS mean velocity profile with vortex sheet. (Right) Magnitude of the Integrand *I* from surface pressure definition.

Figure 16 shows the analysis for a vortex sheet source located at one of the extrema of the mean velocity profile, which in this case corresponds to a location very close to where the canopy would have been located. Fig. 16 (Right, (a)) shows how the integrand is almost a constant zero for this location making its area tend to zero and therefore shielding the wall from surface pressure fluctuations compared to a source that would be located at the same height for the linear profile. Furthermore, at a higher nondimensional frequency as the one seen in Fig. 16 (Right, (b)), the area under the integrand is still very close to zero and smaller compared to the linear profile so the flow at this height will have a very low sensitivity.

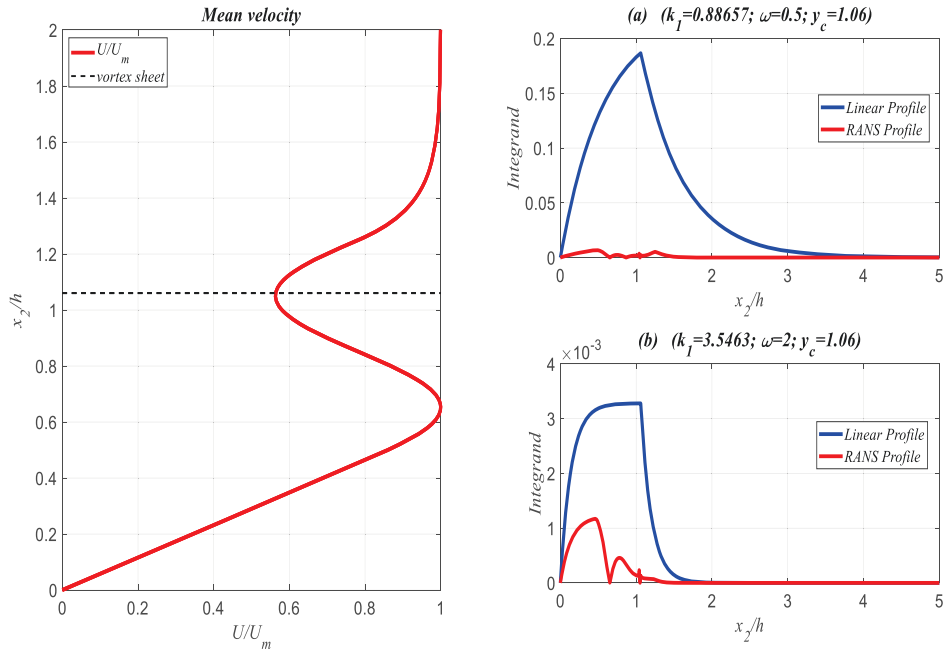

Fig. 16 (Left) Approximation of Gonzalez et al. RANS mean velocity profile with vortex sheet. (Right) Magnitude of the Integrand *I* from surface pressure definition.

Therefore, we can conclude that for this mean velocity profile, there are two very low sensitivity regions that correspond with the extrema of the mean velocity profile. Furthermore, underneath the extrema points, there are regions of low sensitivity at the low frequencies but also of high sensitivity at the higher frequencies.

V. Discussion & Conclusion

We have demonstrated that changing the mean velocity profile influences the surface pressure fluctuations. This occurs because the mean velocity profile affects the unsteady part of the flow. Changing the profile can translate into a more rapid decay of the stream function that defines the unsteady part of the flow reducing the rate of change of the stream function under a particular vortex sheet source if compared to the solution that would be obtained from a linear profile. This effect would translate into shear sheltering and pressure shielding at particular frequencies. However, there are also frequencies and vortex heights were a profile with greater shear increases the rate of change of the stream function under the vortex sheet source when compared to the linear profile, showing regions in the flow where the turbulence level is greater than what it would be for a linear profile. These frequencies and vortex sheets would translate into shear amplification giving a greater level of surface pressure fluctuations.

Therefore, every flow, will show regions of high sensitivity that might appear at some particular frequencies for one specific mean velocity profile but that will change for different velocity profile. The model that we presented here allow us to predict the sensitivity contour of the flow which could help define the velocity profile that is the most suitable or beneficial for the mitigation of trailing edge noise for any particular application.

It is important to note that in this model we have assumed the vortex sheet strength to be constant for all mean velocity profiles analyzed without taking into consideration the effect that the turbulent kinetic energy could have on its magnitude. Therefore, further analysis needs to be carried out in future studies to evaluate the veracity of the assumption of a constant vortex sheet strength as well as the inclusion of the effect of the turbulent kinetic energy.

Acknowledgments

The authors would like to thank the National Science Foundation, in particular Dr. Ron Joslin, for their support of this research under grant CBET-1802915. The assistance of and insightful discussions with Alexander Gonzalez, and Nandita Hari are gratefully acknowledged.

References

[1] Clark, I.A., Alexander, W. N.,Devenport,W.,Glegg,S.,Jaworski,J.W.,Daily,C. and Peake,N. (2017). Bio inspired Trailing-Edge Noise Control. *AIAA Journal* 55(3): 740-754.

[2] Gonzalez, Alexander & Glegg, Stewart & Hari, Nandita & Devenport, William. (2019). Fundamental Studies of the Mechanisms of Pressure Shielding. *AIAA Journal* 10.2514/6.2019-2403.

[3] Shi, Yuejun & Lee, Seongkyu. (2018). Numerical Study of 2-D Finlets Using RANS CFD for Trailing Edge Noise Reduction. *AIAA Journal* 10.2514/6.2018-2812.

[4] Grosch, C.E. and Salwen, H., 1978, The continuous spectrum of the Orr Sommerfeld equation, Part 1, *J. Fluid Mech.* 87(1), 33-54.

[5] Jacobs, R.G., and Durbin, P.A., 1998, Shear sheltering and the continuous spectrum of the Orr =-Sommerfeld equation, Phys. Fluids 10(8), 2006-2011

[6] Hunt, J.C.R., and Durbin, P.A., 1999, Perturbed vortical layers and shear sheltering, Fluid Dyn. Res. 24, 375-404

[7] Lilley, G. (1998). A Study of the Silent Flight of the Owl. AIAA Paper. 9. 10.2514/6.1998-2340.

[8] Finnigan, John. (2000). Turbulence in plant canopies. *Ann Rev Fluid Mech*. Annual Review of Fluid Mechanics. 32. 519-571. 10.1146/annurev.fluid.32.1.519.

[9] Raupach, Michael & Finnigan, John & Brunet, Y. (1996). Coherent Eddies and Turbulence in Vegetation Canopies: The Mixing-Layer Analogy. Boundary-Layer Meteorology. 78. 351-382. 10.1007/978-94-017-0944-6_15.

[10] Amiet, R.K. (1975) Acoustic Radiation from an Airfoil in a Turbulent Stream. Journal of Sound and Vibration, 407- 420.

[11] Ffowcs-Williams and Hall (1969) Aerodynamic sound generation by turbulent flow in the vicinity of a scattering half plane, J. Fluid Mech. 40 (1970) 657–670.

[12] Glegg, S., Devenport, W. Aeroacoustics of low mach number flows, Chippendham: Joe Hayton, 2017.

[13] Drazin, P. / Reid, W., Hydrodynamic Stability. Cambridge, Cambridge University Press 1981. XI

[14] Bodling, A. and Sharma, A. (2018). "Numerical investigation of low-noise airfoils inspired by the down coat of owls". Bioinspiration & Biomimetics. 14. 10.1088/1748-3190/aaf19c.